

## Steering the Nuclear Motion in Singly Ionized Argon Dimers with Mutually Detuned Laser Pulses

J. Wu,<sup>1,2</sup> M. Magrakvelidze,<sup>3</sup> A. Vredenberg,<sup>1</sup> L. Ph. H. Schmidt,<sup>1</sup> T. Jahnke,<sup>1</sup> A. Czasch,<sup>1</sup> R. Dörner,<sup>1,\*</sup> and U. Thumm<sup>3,†</sup>

<sup>1</sup>*Institut für Kernphysik, Goethe-Universität, Max-von-Laue-Strasse 1, D-60438 Frankfurt, Germany*

<sup>2</sup>*State Key Laboratory of Precision Spectroscopy, East China Normal University, Shanghai 200062, China*

<sup>3</sup>*James R. Macdonald Laboratory, Physics Department, Kansas State University, Manhattan, Kansas 66506, USA*

(Received 25 June 2012; published 18 January 2013)

We demonstrate that the vibrational nuclear motion of singly ionized argon dimers can be controlled with two ultrashort laser pulses of *different* wavelengths. In particular, we observe a striking “gap” in the pump-probe-delay-dependent kinetic-energy release spectrum only if the probe-pulse wavelength exceeds the pump-pulse wavelength. This “frustrated dissociation effect” is reproduced by our two-state quantum mechanical model, validating its interpretation as a pump-pulse-initiated population transfer between dipole-coupled Born-Oppenheimer electronic states of the dissociating  $\text{Ar}_2^+$  molecular ion. Our numerical results also reproduce the measured collapse and fractional revival of the oscillating  $\text{Ar}_2^+$  nuclear wave packet, and, for single-pulse dissociation, the decrease of the kinetic-energy release with increasing laser wavelength.

DOI: [10.1103/PhysRevLett.110.033005](https://doi.org/10.1103/PhysRevLett.110.033005)

PACS numbers: 32.80.Rm, 42.50.Hz, 42.65.Re

Comprehensive imaging of electronic or nuclear wave packets is a fundamental prerequisite for a detailed understanding of chemical bond formation and breaking, and a significant step towards the controlled manipulation of chemical reactions with intense pulses of electromagnetic radiation. Ultrashort laser pulses are a powerful tool for such attempts that has enabled the pump-probe-spectroscopic imaging of the spatiotemporal motion of nuclear wave packets in  $\text{H}_2^+$  and  $\text{D}_2^+$  [1–8] and, more recently, in heavier diatomic molecules with several binding electrons [9,10].

In contrast to strongly covalently bound molecules, rare gas dimers and their singly charged cations are very weakly bound. Their large vibrational periods, exceeding those of  $\text{N}_2$ ,  $\text{O}_2$ , and  $\text{CO}$  [9,10] by an order of magnitude, and comparatively simple electronic structure make them ideal, yet to date unexplored, targets for the detailed scrutiny of their bound and dissociating nuclear dynamics near light-induced avoided crossings of Born-Oppenheimer (BO) nuclear potential curves in pump-probe experiments with infrared laser pulses. The low-lying electronic structure of  $\text{Ar}_2^+$ , in particular, has been examined in *ab initio* quantum-chemical calculations and is characterized by six adiabatic electronic states [11–13]. The electronic and rovibrational ground state of  $\text{Ar}_2^+$  is bound with a dissociation energy of 1.34 eV with the equilibrium internuclear distance  $R_0^+ = 4.5$  [12] which is smaller than the ground-state equilibrium distance  $R_0 = 7.2$  of neutral  $\text{Ar}_2$  [14,15] (Unless indicated otherwise, atomic units are used throughout this Letter).

Here, we use ultrashort pump and probe laser pulses of different central frequencies to steer and a typical pump-probe spectroscopy setup [5,9,10,16] to trace the nuclear motion in  $\text{Ar}_2^+$  by measuring the fragment

kinetic-energy release (KER) as a function of time. We probe the evolution of nuclear vibrational wave packets from the bound ground state of  $\text{Ar}_2^+$  to a dissociative state that is populated by one-photon dipole transitions induced in either pump or probe pulse, leading to  $\text{Ar}_2^+ \rightarrow \text{Ar}^+ + \text{Ar}$  dissociation, which we will refer to as the  $\text{Ar}_2(1,0)$  dissociation channel [17–19]. Possible dissociative ionization paths and the relevant dipole-coupled BO potential curves of  $\text{Ar}_2^+$  are shown in Fig. 1. A coherent nuclear wave packet is launched on the  $I(1/2)_u$  potential curve of  $\text{Ar}_2^+$  at  $R_0$  (point A). In Franck-Condon approximation, the heavy nuclei are assumed to be frozen during the ultrafast ionization process [20,21]. In contrast to the well-studied dissociative ionization of  $\text{H}_2$  [5–7], the created vibrational nuclear wave packet of  $\text{Ar}_2^+$  starts to move inwards at point A on the  $I(1/2)_u$  curve since  $R_0^+ < R_0$ . Depending on the central frequency of the laser pulse,  $\omega_l$  or  $\omega_s$ , the wave packet may undergo a dipole-allowed one-photon transition to the  $II(1/2)_g$  curve at points B or C, respectively, followed by  $\text{Ar}_2(1,0)$  dissociation. The final fragment KER is given by the difference of the nuclear potential energies  $V_{u,g}$  in the  $I(1/2)_u$  and  $II(1/2)_g$  states and the photon energy by  $\text{KER}(\omega_{l,s}) = V_u(R_0) - V_g(R = \infty) + \omega_{l,s}$ .

Our measurements were performed using a COLd target recoil ion momentum spectroscopy reaction microscope [22]. Neutral  $\text{Ar}_2$  was generated from a collimated supersonic gas jet and ionized by linearly polarized laser pulses at various wavelengths. A Ti:sapphire laser system was used to generate 780 nm pulses that were split into a pump and probe pulse. One pulse was sent to a traveling-wave optical parametric amplifier to vary its wavelength. The time delay between the pump and probe pulse was controlled by using a motorized translation stage with a

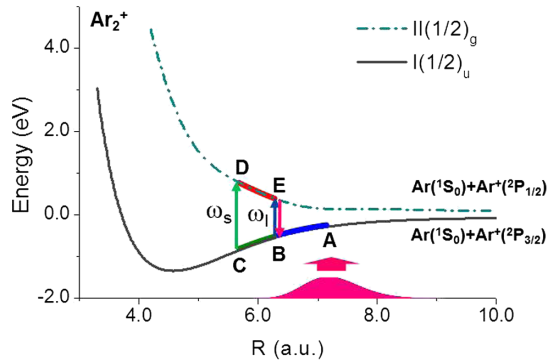


FIG. 1 (color online). Sketch of the  $\text{Ar}_2^+$  dissociation dynamics in two mutually delayed and detuned ultrashort laser pulses with central frequencies  $\omega_s$  and  $\omega_l$  that allow resonant one-photon transitions at internuclear distances  $R$  indicated by  $C$ ,  $D$  and  $B$ ,  $E$ , respectively. The red profile shows the nuclear probability density of the  $\text{Ar}_2$  ground state.

step size of 10 fs. The 3D momenta and KER of the  $\text{Ar}^+$  ions from ionization and dissociation events were reconstructed from the detected times of flight and positions of the charged particles.

Figure 2(a) shows the measured KER spectra in the  $\text{Ar}_2(1,0)$  channel, created by single 60 fs laser pulses with wavelengths between 600 and 1450 nm. In this case, the leading part of the pulse serves as the pump and creates a wave packet on the  $I(1/2)_u$  curve by singly ionizing  $\text{Ar}_2$ , while the remainder of the pulse couples the wave packet to the  $II(1/2)_g$  curve, leading to  $\text{Ar}_2(1,0)$  dissociation. For example, using a single 780 or 1450 nm pulse, only a single peak centered at 1.18 or 0.45 eV, respectively, is observed in the KER spectrum. The KER spectra are fitted to Gaussians to obtain the KER values at maximal yields shown as open squares in Fig. 2(b). These agree well with the expected values (open circles) of  $\text{KER}(\omega)$  for one-photon induced  $\text{Ar}_2(1,0)$  dissociation [17–19]. Using different wavelengths for the pump and probe pulse, the measured KER thus allows us to clearly distinguish the probe-induced signal from the pump-produced background. According to Ref. [18], several electronic states of  $\text{Ar}_2^+$  might be involved in the dissociative single ionization. Subsequently, by using intense fs laser pulses for both ionization and dissociation, the fine-structure split  $I(1/2)_u$  and  $II(1/2)_g$   $\text{Ar}_2^+$  states were found to dominate the dissociation dynamics [19]. This conclusion is confirmed by our good agreement between the measured and expected KERs in Fig. 2(b).

In contrast to light molecules that require sub-10 fs few-cycle pulses to resolve the nuclear dynamics in time [5–7], the slow nuclear motion in  $\text{Ar}_2^+$  can be probed with relatively long laser pulses. Figure 3(a) shows the time-dependent KER spectrum measured for the  $\text{Ar}_2(1,0)$  channel with 780 and 1450 nm pump and probe pulses. For positive (negative) delays, the 780 (1450) nm pulse

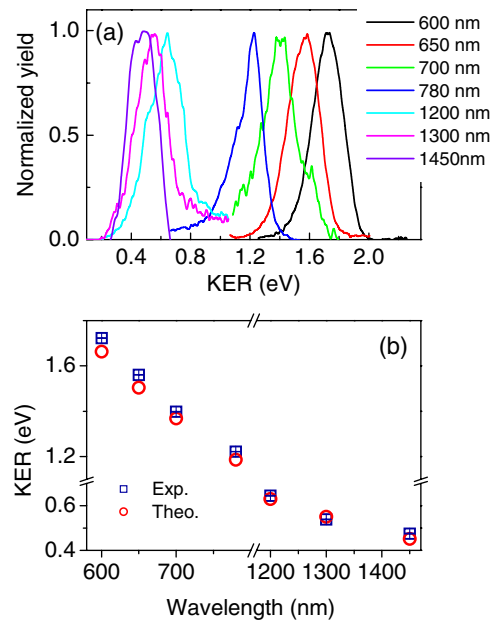


FIG. 2 (color online). (a) Measured KER spectra for  $\text{Ar}_2(1,0)$  in a single 60 fs laser pulse at various wavelengths. (b) Measured and calculated wavelength-dependent KER at the maximal yields in (a).

precedes the 1450 (780) nm pulse. As expected from the discussion of Fig. 2, KERs of both 0.45 and 1.18 eV are observed. Maximal yields for KERs of 0.45 and 1.18 eV occur at delays of  $\sim 11$  fs and  $\sim -18$  fs. The larger delay for finding the maximal yield at 1.18 eV agrees with the larger time needed by the nuclear wave packet in  $\text{Ar}_2^+$  to move from point  $A$  to  $C$  on the  $I(1/2)_u$  potential curve, compared to the time it needs to reach point  $B$  (cf, Fig. 1). The largest intensity at 0.45 eV KER thus appears if the 1450 nm probe pulse is slightly delayed with respect to the 780 nm pump pulse, while 1.18 eV are most efficiently released if the 780 nm probe pulse is slightly delayed relative to the 1450 nm pump pulse. We note that the relative intensities at different KERs in Fig. 3(a) are affected by the need of reducing unavoidable unphysical noise at the lowest KERs.

For negative delays, part of the wave packet couples in the 1450 nm pump pulse at  $B$  to the  $II(1/2)_g$  curve and transits via a dipole-allowed resonant one-photon absorption to point  $E$ , before dissociating along the  $II(1/2)_g$  curve, leading to the measured faint band of time-independent KERs near 0.45 eV. The remaining bound wave packet propagates inwards, is reflected at the repulsive side of the  $I(1/2)_u$  curve, and continues to oscillate in the  $I(1/2)_u$  state. The delayed 780 nm probe pulse destructively images this oscillatory motion of the bound wave packet by dipole-allowed coupling to the  $II(1/2)_g$  curve through a one-photon transition from point  $C$  to  $D$ , followed by dissociation along the  $II(1/2)_g$  curve. With respect to earlier studies [5–7,9,10,16] in which the pump and probe pulses

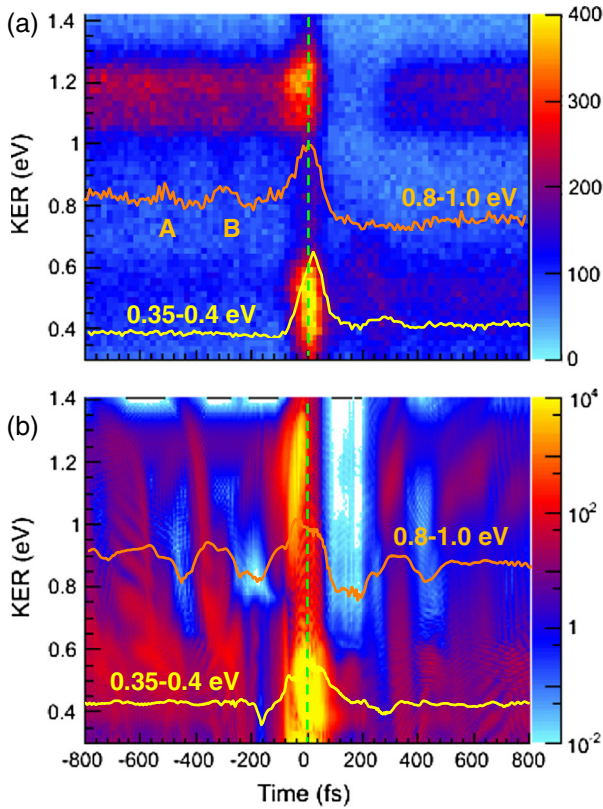


FIG. 3 (color online). (a) Measured  $\text{Ar}_2(1,0)$  KER spectrum as a function of the pump-probe time delay for 60 fs laser pulses with a peak intensity of  $10^{14}$  W/cm $^2$ . (b) Corresponding calculated KER spectrum. The green dashed vertical line indicates zero time delay. The orange and yellow curves labeled with 0.8–1.0 eV and 0.35–0.4 eV are partial fragment yields obtained by integrating the spectra in (a) and (b) over the KER ranges from 0.8 to 1.0 eV and 0.35 to 0.4 eV, respectively.

have the same wavelengths, using pulses of different wavelengths allows us to map the oscillatory nuclear motion to a different KER that can be readily distinguished. Indeed, as shown in Fig. 3(a) for negative delays, several tilted weak stripes extend from the KER band near 1.18 eV to the one near 0.45 eV. To better display this measured oscillation, the orange upper curve in Fig. 3(a) shows the time-dependent KER spectrum integrated from 0.8 to 1.0 eV. The two weak humps at negative delays, labeled as A and B on this curve are separated by approximately the vibrational period of  $\text{Ar}_2^+$  in the  $I(1/2)_u$  state ( $\sim 270$  fs). Similarly, but less obviously, the oscillatory motion is imaged for positive delays, where the nuclear wave packet launched by the 780 nm pump pulse dissociates following the action of the delayed 1450 nm probe pulse. This is better seen after integrating the time-dependent KER spectrum from 0.35 to 0.4 eV [yellow lower curve in Fig. 3(a)].

In addition to the expected vibrational structure in the band of KERs near 0.45 eV, a “delay gap” is observed in the band of KERs near 1.18 eV in Fig. 3(a). This gap occurs only for positive delays, extends over a delay range of

approximately 200 fs, and is consistent with the following frustrated- $II(1/2)_g$ -dissociation mechanism. The  $\text{Ar}_2^+$  nuclear wave packet launched by the 780 nm pump pulse propagates inwards from A to C on the  $I(1/2)_u$  curve and transits to D on the  $II(1/2)_g$  curve by absorbing one photon in the pump pulse (cf., Fig. 1). During its subsequent outwards propagation on the  $II(1/2)_u$  curve, the wave packet is effectively coupled back to the  $I(1/2)_u$  curve at E by the one-photon-resonant 1450 nm probe pulse. The dissociation of the nuclear wave packet initiated on the  $II(1/2)_g$  curve by the 780 nm pump pulse is thus cut short by the time-delayed 1450 nm probe pulse. This downward transfer of the dissociating wave packet from the repulsive  $II(1/2)_g$  curve to the bound  $I(1/2)_u$  curve does not occur if the probe pulse arrives after the wave packet has completely passed point E. Therefore, the band of KERs near 1.18 eV reappears at larger positive delays. This delay gap is not observed for negative delays since the dissociating wave packet created on the repulsive  $II(1/2)_g$  curve by the 1450 nm pump pulse at E propagates outwards and will never reach D where it could be down-converted to the  $I(1/2)_u$  curve by the 780 nm probe pulse in a dipole-allowed resonant one-photon transition.

In order to confirm the above interpretation of our experimental observations, we numerically propagate the vibrational nuclear wave packet by solving the time-dependent Schrödinger equation in the subspace of the  $I(1/2)_u$  and  $II(1/2)_g$  states of  $\text{Ar}_2^+$  [21]. To simulate ionization and dissociation by each laser pulse, we employ internuclear-distance-dependent molecular Ammosov-Delone-Krainov (ADK) rates [21] and coherently seed the wave packet on the  $I(1/2)_u$  state by depleting the ground state of neutral  $\text{Ar}_2$ . While propagating the wave packet we allow for dipole couplings to the  $II(1/2)_g$  state in either one of the two pulses. After the end of the probe pulse, the wave packet is allowed to freely propagate for a sufficiently long time ( $\sim 500$  fs), when the bound part of the wave packet becomes separable from the dissociating part. We then Fourier transform the dissociating parts of the wave packet for internuclear distances between 10 and 160 a.u. to obtain its momentum distribution and the KER spectrum [9].

Figure 3(b) shows our calculated time-delay-dependent KER spectrum, focal-volume averaged [23] over intensities between  $10^{12}$  and  $10^{14}$  W/cm $^2$ . The numerical simulation reproduces several features of the experimental data in Fig. 3(a), such as the strong enhancement of the dissociation yield near zero time delay and (for both positive and negative delays) the periodic stripes that map the oscillation of the vibrational wave packet on the  $I(1/2)_u$  potential curve. Most importantly, the frustrated dissociation effect, i.e., the delay gap in the band of KERs near 1.18 eV for positive delays is reproduced in the calculation. Numerical tests showed that this gap also occurs at different combinations of wavelengths (600/1200 nm, 790/1000 nm, and 790/1800 nm), as long as the wavelengths of pump and

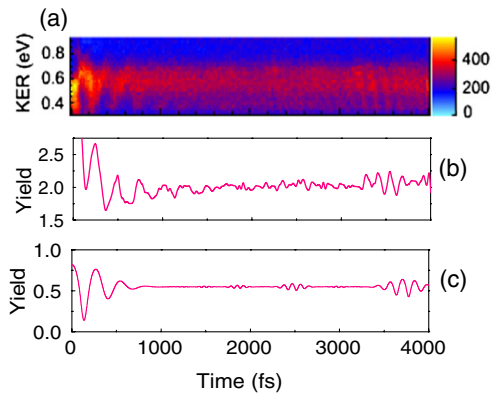


FIG. 4 (color online). (a) Measured time-dependent KER spectrum as in Fig. 3(a), but for an increased pump-pulse peak intensity of  $9 \times 10^{14}$  W/cm<sup>2</sup> and an extended delay range. (b) Dissociation yield obtained by integration over the KER range in (a). (c) The calculated dissociation yield for the same KER range.

probe pulse is sufficiently different for the resulting two bands of KERs to remain distinguishable. Two pulses of different wavelength can thus be used as a gate, either allowing or terminating the previously initiated dissociation along a specific adiabatic molecular potential curve.

By increasing the intensity of the pump pulse and the delay range, we observe not only the vibrational motion of the nuclear wave packet but also its revival at around 3.5 ps [Fig. 4(a)]. Figure 4(b) shows the dissociation yield obtained by integrating over the KER range in Fig. 4(a). The Ar<sub>2</sub><sup>+</sup> nuclear wave packet created by the pump pulse decoheres after about four vibrational periods. The imaged oscillation period near delays of 3.5 ps is  $\sim 140$  fs, which is roughly half of the fundamental oscillation period of the nuclear wave packet, indicating a *half* revival in which the oscillation frequency is doubled due to two counterpropagating daughter wave packets [24]. Indeed, by fitting the  $I(1/2)_u$  curve with a Morse potential, we determined the full revival time from the Morse-potential parameters [9] as  $\sim 7.4$  ps. Figure 4(c) shows the corresponding calculated revival structure.

In summary, by using the weakly bound Ar<sub>2</sub><sup>+</sup> as a clean system with a few well-known potential energy curves, we have probed the oscillation, dephasing, and revival of its nuclear vibrational wave packet. Using a two-color pump-probe scheme to distinguish the KER spectrum of the signal from the pump background, we identified for the first time a frustrated dissociation mechanism in Ar<sub>2</sub><sup>+</sup> and showed that the dissociation path of a dissociating nuclear wave packet that was created by the shorter-wavelength pump pulse can be efficiently controlled by tuning the time delay of a longer-wavelength probe pulse. The interpretation of our experimental data is validated by the results of our two-state quantum simulation.

We acknowledge stimulating discussions with T. Pfeifer and R. Moshhammer. This work was supported by a Koselleck

Project of the Deutsche Forschungsgemeinschaft. J.W. acknowledges support by the Alexander von Humboldt Foundation. M.M. and U.T. were supported in part by the Chemical Sciences, Geosciences, and Biosciences Division, Office of Basic Energy Sciences, Office of Science, U.S. DOE and U.S. NSF Grant No. PHY 1068752.

\*doerner@atom.uni-frankfurt.de

†thumm@phys.ksu.edu

- [1] M. Kremer, B. Fischer, B. Feuerstein, V.L.B. de Jesus, V. Sharma, C. Hofrichter, A. Rudenko, U. Thumm, C.D. Schröter, R. Moshhammer, and J. Ullrich, *Phys. Rev. Lett.* **103**, 213003 (2009).
- [2] D. Ray, F. He, S. De, W. Cao, H. Mashiko, P. Ranitovic, K.P. Singh, I. Znakovskaya, U. Thumm, G.G. Paulus, M.F. Kling, I.V. Litvinyuk, and C.L. Cocke, *Phys. Rev. Lett.* **103**, 223201 (2009).
- [3] G. Sansone, F. Kelkensberg, J.F. Pérez-Torres, F. Morales, M.F. Kling, W. Siu, O. Ghafur, P. Johnsson, M. Swoboda, E. Benedetti, F. Ferrari, F. Lépine, J.L. Sanz-Vicario, S. Zherebtsov, I. Znakovskaya, A. L'Huillier, M. Yu. Ivanov, M. Nisoli, F. Martin, and M.J.J. Vrakking, *Nature (London)* **465**, 763 (2010).
- [4] K.P. Singh, F. He, P. Ranitovic, W. Cao, S. De, D. Ray, S. Chen, U. Thumm, A. Becker, M.M. Murnane, H.C. Kapteyn, I.V. Litvinyuk, and C.L. Cocke, *Phys. Rev. Lett.* **104**, 023001 (2010).
- [5] Th. Ergler, A. Rudenko, B. Feuerstein, K. Zrost, C.D. Schröter, R. Moshhammer, and J. Ullrich, *Phys. Rev. Lett.* **97**, 193001 (2006).
- [6] B. Feuerstein, Th. Ergler, A. Rudenko, K. Zrost, C.D. Schröter, R. Moshhammer, J. Ullrich, T. Niederhausen, and U. Thumm, *Phys. Rev. Lett.* **99**, 153002 (2007), and references therein.
- [7] I.A. Bocharova, H. Mashiko, M. Magrakvelidze, D. Ray, P. Ranitovic, C.L. Cocke, and I.V. Litvinyuk, *Phys. Rev. A* **77**, 053407 (2008).
- [8] M. Winter, R. Schmidt, and U. Thumm, *Phys. Rev. A* **80**, 031401 (2009).
- [9] S. De, I.A. Bocharova, M. Magrakvelidze, D. Ray, W. Cao, B. Bergues, U. Thumm, M.F. Kling, I.V. Litvinyuk, and C.L. Cocke, *Phys. Rev. A* **82**, 013408 (2010); S. De, M. Magrakvelidze, I.A. Bocharova, D. Ray, W. Cao, I. Znakovskaya, H. Li, Z. Wang, G. Laurent, U. Thumm, M.F. Kling, I.V. Litvinyuk, I. Ben-Itzhak, and C.L. Cocke, *Phys. Rev. A* **84**, 043410 (2011).
- [10] I.A. Bocharova, A.S. Alnaser, U. Thumm, T. Niederhausen, D. Ray, C.L. Cocke, and I.V. Litvinyuk, *Phys. Rev. A* **83**, 013417 (2011).
- [11] F.X. Gadea and I. Páidarová, *Chem. Phys.* **209**, 281 (1996).
- [12] T.-K. Ha, P. Rupper, A. Wüest, and F. Merkt, *Mol. Phys.* **101**, 827 (2003).
- [13] W.J. Stevens, M. Gardner, A. Karo, and P. Julienne, *J. Chem. Phys.* **67**, 2860 (1977).
- [14] K. Patkowski, G. Murdachaew, C.-M. Fou, and K. Szalewicz, *Mol. Phys.* **103**, 2031 (2005), and references therein.

- [15] S.D. Stoychev, A.I. Kuleff, F. Tarantelli, and L.S. Cederbaum, *J. Chem. Phys.* **128**, 014307 (2008).
- [16] T. Baumert, V. Engel, C. Meier, and G. Gerber, *Chem. Phys. Lett.* **200**, 488 (1992).
- [17] M. Magrakvelidze, F. He, T. Niederhausen, I.V. Litvinyuk, and U. Thumm, *Phys. Rev. A* **79**, 033410 (2009), and references therein.
- [18] C. Wunderlich, H. Figger, and T. W. Hänsch, *Phys. Rev. A* **62**, 023401 (2000), and references therein.
- [19] J. Wu, A. Vredenburg, B. Ulrich, L.Ph.H. Schmidt, M. Meckel, S. Voss, H. Sann, H. Kim, T. Jahnke, and R. Dörner, *Phys. Rev. A* **83**, 061403(R) (2011).
- [20] U. Thumm, T. Niederhausen, and B. Feuerstein, *Phys. Rev. A* **77**, 063401 (2008).
- [21] T. Niederhausen and U. Thumm, *Phys. Rev. A* **77**, 013407 (2008); T. Niederhausen, U. Thumm, and F. Martin, *J. Phys. B* **45**, 105602 (2012).
- [22] J. Ullrich, R. Moshhammer, A. Dorn, R. Dörner, L. Ph. H. Schmidt, and H. Schmidt-Böcking, *Rep. Prog. Phys.* **66**, 1463 (2003).
- [23] M. Magrakvelidze, C.M. Aikens, and U. Thumm, *Phys. Rev. A* **86**, 023402 (2012).
- [24] R.W. Robinett, *Phys. Rep.* **392**, 1 (2004).